Signatures of vibrational interactions in coherent two-dimensional infrared spectroscopy

ARTICLE *in* CHEMICAL PHYSICS · MAY 2001

Impact Factor: 1.65 · DOI: 10.1016/S0301-0104(01)00230-0

2 AUTHORS:

Munira Khalil
University of Washington Seattle
59 PUBLICATIONS **2,246** CITATIONS
SEE PROFILE

Andrei Tokmakoff
University of Chicago
153 PUBLICATIONS **8,075** CITATIONS
SEE PROFILE

ELSEVIER

Chemical Physics 266 (2001) 213–230

Chemical Physics

www.elsevier.nl/locate/chemphys

Signatures of vibrational interactions in coherent two-dimensional infrared spectroscopy

M. Khalil, A. Tokmakoff *

Department of Chemistry, Massachusetts Institute of Technology, Cambridge, MA 02139, USA

Received 17 October 2000

Abstract

The influence of three vibrational interaction mechanisms on two-dimensional (2D) spectra derived from infrared (IR) photon echo experiments is investigated. In particular it is shown that the existence of a nonlinear signal requires one of the following vibrational nonlinearities: (1) anharmonicity in the ground state potential, (2) nonlinear dependence of the transition dipole moment on the vibrational coordinates, or (3) level-dependent dephasing dynamics. 2D spectra arising from these interactions are investigated using a model of two coupled cubic anharmonic oscillators. The third-order nonlinear response for this model arises from 20 different vibronic coherence pathways involving six possible vibrational states. It is shown that the three interaction mechanisms are revealed by distinct signatures in the 2D spectrum: the positions, amplitudes, and shape of peaks, respectively. These signatures provide an intuitive framework for the analysis of 2D IR spectra.

1. Introduction

Vibrational spectroscopy is particularly powerful as a tool for probing both molecular structure and dynamics. Vibrational transitions probe well-defined molecular coordinates, and the study of fundamental, overtone and combination band transition frequencies carries information on the ground state nuclear potential and molecular structure. Vibrational line shapes carry information on energy, phase, and orientational relaxation processes. While such information is required to understand molecular structure, chemical reactions, and physical processes in condensed phases, traditional linear vibrational spectroscopy of these systems is generally ambiguous. In systems where multiple degrees of freedom interact and evolve simultaneously over multiple time scales, molecular information in a linear, one-dimensional (1D) vibrational spectrum, is masked by spectral congestion and featureless line shapes, obscured combination and overtone bands, and static and/or dynamic line broadening. The term 1D refers to the single frequency axis over which spectral data is presented, or equivalently, the single time variable in the correlation function describing these experiments. The inadequacy of traditional linear spectroscopy for obtaining information on specific molecular interactions has motivated the development of multi-dimensional, nonlinear vibrational spectroscopies. These include the infrared (IR) photon echo (PE) [1–4], the Raman echo [5,6],

* Corresponding author. Tel.: +1-617-253-4503; fax: +1-617-253-7030.

E-mail address: tokmakof@mit.edu (A. Tokmakoff).

0301-0104/01/$ - see front matter
PII: S0301-0104(01)00230-0

transient IR pump–probe [7,8], and IR-pump/Raman-probe experiments [9], which allow various contributions to the vibrational line shape to be dissected, and give insight into vibrational couplings. These methods are formally described in terms of multi-time correlation functions, which represent measurements in a higher dimensionality.

Since there are clear analogies between nonlinear vibrational spectroscopies and the two-dimensional (2D) methods in nuclear magnetic resonance (NMR) [10], there is interest in developing the former into coherent multi-dimensional techniques [11,12]. Analogous to the study of coupled spin systems with 2D NMR, coherent 2D vibrational spectroscopies have the potential to observe and quantify vibrational couplings and interactions, and to separate and measure vibrational line-broadening mechanisms. These are precisely the types of observables that would allow for an effective characterization of the potential energy surface of a condensed phase system. Furthermore, with insight into the type of interaction mechanism giving rise to 2D IR spectra, there is potential for using couplings to extract molecular structural information on the time scale of the homogeneous vibrational line widths, i.e. 1–10 ps.

These observations have led to numerous theoretical and experimental investigations into methods of obtaining and interpreting 2D vibrational spectra [12]. 2D Raman spectroscopy [13] based on a fifth-order nonlinearity was initially proposed [14] and developed as a method for probing inhomogeneous broadening of collective intermolecular motions, but its sensitivity to various vibrational coupling mechanisms also led to its use in observing couplings between localized high frequency modes [15]. A number of experimental 2D Raman studies suggested that there were three types of vibrational interaction effects that would lead to observing a 2D signal: vibrational anharmonicity, nonlinearity of the polarizability, and quantum-level-dependent dephasing [13–17]. Distinguishing and understanding these interactions leads to recipes for observing transient molecular structure, for instance through dipole-induced-dipole interactions [18]. Experimentally, the use of this method is complicated by the need to suppress cascaded optical nonlinearities in the signal. Various methods are currently being explored to address this issue [19–21].

2D IR methods are simultaneously being developed for obtaining similar types of information. Dispersed IR pump–probe [22,23], dispersed IR PE [24,25], and double vibrationally enhanced IR spectroscopy [26] are third-order nonlinear techniques in which the nonlinear signal is sampled in two time or frequency dimensions to better observe vibrational couplings and characterize inhomogeneous broadening. To create a vibrational analog of 2D Fourier transform NMR, 2D vibrational experiments with phase-sensitive detection are required in which the creation and evolution of vibrational coherences for a system of coupled vibrations can be monitored [24,27]. By temporally or spectrally characterizing the radiated nonlinear signal field as a function of time delays between input pulses, a 2D response can be observed and represented as a 2D Fourier transform spectrum. The diagonal peaks in such a spectrum (where the frequency arguments are the same) characterize the dynamics of individual vibrational coordinates of the system, whereas cross-peaks between the diagonal features represent couplings between vibrations. While several methods have been proposed, 2D IR PE techniques using heterodyne detection are perhaps the most intuitive and most powerful of such methods for quantifying the strength and time scale of couplings between different vibrational degrees of freedom, and distinguishing inhomogeneous broadening.

With the development of multi-dimensional spectroscopic methods it becomes necessary to understand the vibrational interactions that give rise to a 2D vibrational spectrum. The varying ways in which the vibrational modes of a system can interact raises several questions. How do the different vibrational couplings manifest themselves in a 2D spectrum? Do these mechanisms have distinct signatures in a 2D map? And perhaps, more importantly, can we identify a microscopic basis for their existence? The aim of this paper is to elucidate the vibrational interactions that give rise to coherent 2D IR signals in general, and, in particular to describe these effects in a 2D heterodyne-detected PE spectrum using a model of anharmonically coupled oscillators. Inhomogeneous

broadening and orientational effects are not considered here.

It is well known that for a particular fundamental vibration to be IR active and reveal itself in a linear 1D spectrum, its vibrational motion must cause a change in the permanent dipole moment ($\partial\mu/\partial q \neq 0$). This condition forms a selection rule for linear spectroscopy. To observe a signal from nonlinear vibrational spectroscopic techniques, such as the 2D experiments discussed here, other considerations also apply. It is well understood that the nonlinear optical response from a set of harmonic oscillators vanishes due to destructive interference between coherences involving adjacent vibrational levels. Thus observing a nonlinear signal requires a deviation from harmonic behavior. In particular, we will show that one of the following conditions must be fulfilled to observe a 2D spectrum: (1) anharmonicity in the ground state potential, (2) nonlinear dependence of the transition dipole on vibrational coordinates, or (3) level-dependent dephasing dynamics. This set of conditions represents three manners of deviation from purely harmonic behavior, and thereby forms a set of selection (or propensity) rules for 2D IR spectroscopy. In this paper we use a model of two oscillators coupled through a cubic anharmonicity to discuss how each of these interaction mechanisms manifest themselves in 2D IR spectra, and how these conditions are related to one another. It is shown that these three vibrational interactions affect the positions, amplitudes and shapes of the various peaks in a 2D spectrum, respectively. These vibrational interactions are in essence the same as those that have been discussed earlier in the context of 2D Raman spectroscopies, where effects of anharmonicity in the ground potential state and the nonlinear polarizability have been examined theoretically and experimentally [14,15,17]. Level-dependent (quantum-number-dependent) dephasing has also been considered, yet not received as much attention [16].

This paper is also motivated by recent theoretical and experimental work on strongly coupled vibrations in 2D IR spectroscopy. In the limit of slow damping of coherences, the nonlinear exciton model for the optical response of two coupled vibrations predicts the existence of 10 peaks arising from transitions involving the one- and two-exciton states [12,28,29]. Here we discuss the source of these peaks using perturbation theory described in terms of the eigenstates of the system. The existence of these 10 peaks has now been experimentally observed in 2D IR PE spectra of the coupled CO stretches of $Rh(CO)_2(C_5H_7O_2)$ in hexane [27].

The paper is organized as follows. Section 2 describes the anharmonically coupled oscillator model, along with the calculation of the nonlinear response for such a system. Section 3 describes each of the three vibrational interactions forming the set of selection rules, in an attempt to catalogue their effects in a 2D spectrum. For a strongly coupled system in the weak damping limit, each type of interaction has a clear manifestation in the 2D absolute value spectrum. Section 4 will discuss the implications of these calculations in understanding 2D spectra of complex systems and suggest rules for analyzing experimental data sets.

2. Nonlinear response of coupled oscillators

2.1. Cubic anharmonic oscillators

To describe the 2D IR spectroscopy of coupled vibrations, we use a system of two oscillators with fundamental frequencies ω_a^0 and ω_b^0 and expand the potential to include cubic anharmonic terms in both coordinates:

$$V(Q_a,Q_b) \cong \tfrac{1}{2}\hbar\omega_a^0 Q_a^2 + \tfrac{1}{2}\hbar\omega_b^0 Q_b^2 + \tfrac{1}{6}\big(g_{aaa}Q_a^3 + g_{bbb}Q_b^3 + 3g_{aab}Q_a^2 Q_b + 3g_{abb}Q_a Q_b^2\big). \quad (1)$$

Here Q_a and Q_b are the reduced vibrational coordinates of the normal coordinates, q_a and q_b:

$$Q_i = \sqrt{\frac{2m_i\omega_i^0}{\hbar}}q_i, \quad (2)$$

where m_i represents the reduced mass of the ith vibrational coordinate. The expansion coefficients, g_{ijk} are the third-order derivatives of the potential surface with respect to its coordinates evaluated at the equilibrium position.

$$g_{ijk} = \left(\frac{\partial^3 V}{\partial Q_i \partial Q_j \partial Q_k} \right)_{Q_0}. \tag{3}$$

Coupling terms are taken to be invariant to the interchange of indices i, j and k, implying that $g_{aab} = g_{aba} = g_{baa}$ and $g_{bba} = g_{bab} = g_{abb}$. The energies of the various vibrational levels can be calculated by perturbation theory [30] to second order in the coupling terms as shown below [31, 32]

$$\begin{aligned} \frac{E_{nk}}{hc} = {} & X_0 + X_a\left(n+\frac{1}{2}\right) + X_b\left(k+\frac{1}{2}\right) \\ & + X_{aa}\left(n+\frac{1}{2}\right)^2 + X_{bb}\left(k+\frac{1}{2}\right)^2 \\ & + X_{ab}\left(n+\frac{1}{2}\right)\left(k+\frac{1}{2}\right). \end{aligned} \tag{4}$$

In the above equation, n and k are the vibrational quantum numbers of the anharmonically coupled vibrations v_a and v_b. The parameters X_i and X_{ij} are related to the anharmonic parameters in the nuclear potential in the following way:

$$X_a = \frac{1}{hc}\left(\hbar\omega_a^0\right), \tag{5a}$$

$$X_b = \frac{1}{hc}\left(\hbar\omega_b^0\right), \tag{5b}$$

$$X_{aa} = \frac{1}{hc}\left(\frac{g_{aab}^2}{2\hbar}\left(\frac{\left(\omega_b^0\right)^2 - 8\left(\omega_a^0\right)^2}{\omega_b^0\left(\left(\omega_b^0\right)^2 - 4\left(\omega_a^0\right)^2\right)} \right) - \frac{5}{6\hbar\omega_a^0} g_{aaa}^2 \right), \tag{5c}$$

$$X_{bb} = \frac{1}{hc}\left(\frac{g_{abb}^2}{2\hbar}\left(\frac{\left(\omega_a^0\right)^2 - 8\left(\omega_b^0\right)^2}{\omega_a^0\left(\left(\omega_a^0\right)^2 - 4\left(\omega_b^0\right)^2\right)} \right) - \frac{5}{6\hbar\omega_b^0} g_{bbb}^2 \right), \tag{5d}$$

$$X_{ab} = \frac{1}{hc}\left(\frac{g_{abb}^2}{\hbar}\left(\frac{4\omega_b^0}{\left(\left(\omega_a^0\right)^2 - 4\left(\omega_b^0\right)^2\right)} \right) + \frac{g_{aab}^2}{\hbar}\left(\frac{4\omega_a^0}{\left(\left(\omega_b^0\right)^2 - 4\left(\omega_a^0\right)^2\right)} \right) \right), \tag{5e}$$

$$X_0 = \frac{1}{hc}\left(-\frac{g_{abb}^2}{8\hbar}\left(\frac{3\omega_a^0}{\left(\left(\omega_a^0\right)^2 - 4\left(\omega_b^0\right)^2\right)} \right) + \frac{g_{aab}^2}{8\hbar}\left(\frac{3\omega_b^0}{\left(4\left(\omega_a^0\right)^2 - \left(\omega_b^0\right)^2\right)} \right) - \frac{7}{72\hbar\omega_a^0} g_{aaa}^2 - \frac{7}{72\hbar\omega_b^0} g_{bbb}^2 \right). \tag{5f}$$

For the purpose of calculating transition dipole moments, the anharmonic eigenstates are obtained by including the first-order corrections to the harmonic wave functions.

2.2. 2D IR photon echo spectrum

IR PE spectroscopy has traditionally been used to extract the homogenous line width from inhomogeneously broadened vibrational spectra and probe spectral diffusion. More generally, Fourier transform 2D IR PE spectroscopy observes the creation and evolution of coherences involving one or more vibrational states, and represents them as a 2D spectrum whose frequency axes describe the preparation and detection period. In a resonant 2D IR PE experiment, three time-ordered fields $\mathbf{E}_1$, $\mathbf{E}_2$, and $\mathbf{E}_3$ generate a nonlinear signal field in the wave-vector direction, $\mathbf{k}_s = -\mathbf{k}_1 + \mathbf{k}_2 + \mathbf{k}_3$. The first pulse excites vibrational coherences for all transitions that lie within the bandwidth of the pulse. During an experimentally controlled time, τ_1, coherences evolve and relax through pure dephasing, population relaxation, and orientational motion. After τ_1, a pair of pulses with wave vectors $\mathbf{k}_2$ and $\mathbf{k}_3$ resonant with the fundamental and higher lying transitions, acts on this evolving coherence, inducing – among other things – coherence transfer to other vibrational states and

rephasing processes. The time evolution of the system in this final coherence state during time τ_3, is described by the third-order polarization, and can be observed by characterizing the amplitude and phase of the radiated nonlinear signal field. A Fourier transform of the evolution of the system in the first and second coherence periods yields a 2D spectrum that provides information about the nature, strength and time scales of coupling between vibrations, as well as the inhomogeneous broadening of those transitions.

A third-order nonlinear experiment measures the convolution of the tensorial third-order response function, $\mathbf{R}^{(3)}$ with the three input electric fields [33]

$$\begin{aligned}\mathbf{P}^{(3)}(\tau_1,\tau_2,t) \propto & \int_0^\infty \mathrm{d}t_3 \int_0^\infty \mathrm{d}t_2 \\ & \times \int_0^\infty \mathrm{d}t_1 \mathbf{R}^{(3)}(t_1,t_2,t_3) \\ & \times \overline{\mathbf{E}}_1(t-t_1-t_2-t_3+\tau_1+\tau_2) \\ & \times \overline{\mathbf{E}}_2(t-t_2-t_3+\tau_2)\overline{\mathbf{E}}_3(t-t_3). \quad (6)\end{aligned}$$

In the above expression, t_1, t_2, and t_3 represent the points at which the input fields interact with the sample within the envelope of the pulses to create the third-order polarization at time t. The variables τ_1 and τ_2 represent the experimentally controlled delays between pulses $\mathbf{E}_1$ and $\mathbf{E}_2$, and between pulses $\mathbf{E}_2$ and $\mathbf{E}_3$, respectively, measured with respect to the center of the pulses. In a heterodyne-detected experiment, the signal field generated from the third-order nonlinear polarization is mixed with a pulsed local oscillator (LO) field to characterize the phase as well as the amplitude of the signal of interest. For phase-locked pulses, where there is a definite relationship between the relative phase (φ) of the signal field and the LO, the detected 2D PE signal can be written as:

$$S(\tau_1,\tau_2,\tau_3,\varphi) \propto \int_{-\infty}^{\infty} \mathrm{d}t\, \mathbf{P}^{(3)}(\tau_1,\tau_2,t)\overline{\mathbf{E}}_{\mathrm{LO}}(t-\tau_3,\varphi), \quad (7)$$

where τ_3 is the experimentally controlled delay between the LO and $\mathbf{P}^{(3)}$. The heterodyned signal can be characterized by measuring a temporal or spectral interferogram [24,34,35]. By controlling the phase of the LO, the complex signal field can be completely characterized. If the pulses are considered to be in the delta function limit, where $t_1 = \tau_1$, $t_2 = \tau_2$ and $t_3 = t$, the fourfold integration in Eqs. (6) and (7) can be carried out trivially and the signal becomes proportional to the third-order response function.

$$S(\tau_1,\tau_2,\tau_3) \propto \mathbf{R}^{(3)}(\tau_1,\tau_2,\tau_3). \quad (8)$$

The response function for a system of anharmonically coupled vibrations can be described using diagrammatic perturbation theory for the evolution of the density matrix, which involves summing over all the possible vibronic interaction pathways. In the rotating wave approximation we consider all processes resonant with the eigenstates present in the one-quantum (singly excited) and two-quantum (doubly excited) manifolds. This approach is analogous to the exciton model of N interacting three-level systems where the three levels include the ground state, a manifold of N one-exciton states, and a manifold of $N(N+1)/2$ two-exciton states [8,12]. The exciton model has been described as a quasiparticle approach and uses the nonlinear exciton equations to model the nonlinear response function. The exciton model has been used to describe nonlinear 2D electronic spectroscopies on photosynthetic complexes, J aggregates and molecular crystals and 2D IR spectroscopies on localized amide I vibrations in dipeptides and small polypeptides [12].

Generally for a system of coupled vibrations, we must consider both the dynamics of the vibrational interactions and relaxation, and the orientation of the dipoles associated with these coordinates in describing the material response. If the dynamics associated with vibrational relaxation processes can be decoupled from orientational dynamics of the molecule, then the third-order response function can be described as

$$\mathbf{R}^{(3)}_{lkji}(\tau_1,\tau_2,\tau_3) = \sum_{\mathrm{vib}} R^{\mathrm{vib}}(\tau_1,\tau_2,\tau_3) R^{\mathrm{or}}_{lkji}(\tau_1,\tau_2,\tau_3). \quad (9)$$

Here, the total response is composed of a vibronic response R^{vib} and orientational response R^{or}_{lkji}

summed over all possible vibronic pathways. The vibronic part contribution is isotropic in nature and describes the vibrational dynamics for a particular sequence of excitations. The orientational response function accounts for the relative orientation of the dipoles of the system, their interactions with the arbitrarily polarized input light fields, and the orientational relaxation processes. It is also dependent on the vibronic pathway. In this paper we focus only on the isotropic vibronic contribution from the two anharmonically coupled oscillators. The orientational contribution and a joint description of the entire response will be the subject of a future publication [36].

Fig. 1 shows an energy level diagram of the six vibrational levels for the two anharmonically coupled oscillators that are relevant to the experiment. In addition to the ground state, the eigenstates $|0,1\rangle$ and $|1,0\rangle$ form the one-quantum manifold, and the three states $|0,2\rangle$, $|2,0\rangle$ and $|1,1\rangle$ constitute the two-quantum manifold. The transition frequencies, ω_{fi}, are defined as:

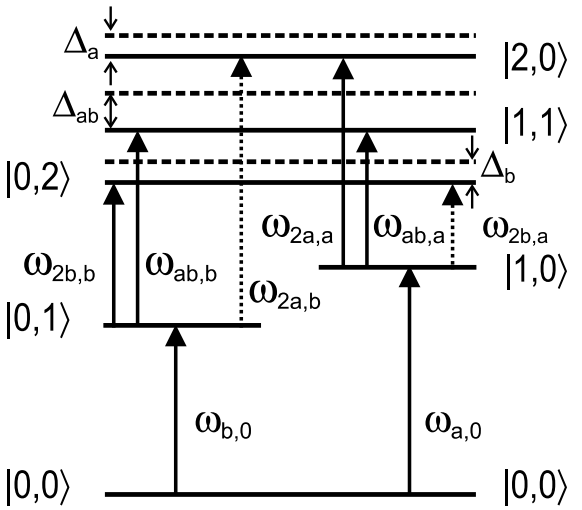

Fig. 1. Energy level structure for two anharmonically coupled vibrations designated as a and b. Shown are the various eigenstates $|n,k\rangle$ where n and k are the respective vibrational quantum numbers for modes a and b. The eigenstates in the two-quantum manifold are red shifted due to the anharmonicity in the nuclear potential by splittings Δ_a, Δ_b and Δ_{ab}. The straight lines show the allowed one-quantum transitions for a harmonic system. The dotted lines show three-quantum transitions that are allowed due to the anharmonicity in the nuclear potential.

$$\omega_{fi} = \frac{E_f - E_i}{\hbar}. \tag{10}$$

The two frequencies, $\omega_{a,0}$ and $\omega_{b,0}$, represent the two fundamental transitions of the coupled modes. These frequencies are shifted from their unperturbed values, ω_a^0 and ω_b^0 because of the anharmonicity in the potential. The anharmonicity also affects the energies of the states in the two-quantum manifold indicated by the energy splittings, Δ_a, Δ_b and Δ_{ab}. Using Eq. (4), these anharmonic splittings can be related to the anharmonic coupling constants, g_{ijk}, through

$$\Delta_a = 2E_{10} - E_{20} = -2X_{aa}, \tag{11a}$$

$$\Delta_b = 2E_{01} - E_{02} = -2X_{bb}, \tag{11b}$$

$$\Delta_{ab} = E_{10} + E_{01} - E_{11} = -X_{ab}. \tag{11c}$$

The incident fields are short pulses with broad bandwidth that spans both fundamental transitions, and is also be resonant with transitions between the one- and two-quantum manifold. The coherences initially excited and observed during τ_1 involve superpositions of ground and one-quantum states. After the remaining excitation fields, the system can evolve during τ_3 by oscillating at either a fundamental frequency, $\omega_{a,0}$ and $\omega_{b,0}$, or it can oscillate in a coherence involving superpositions of the one- and two-quantum states. These are the remaining transitions pictured in Fig. 1, with the following six frequencies: $\omega_{2a,a} = \omega_{a,0} - \Delta_a$, $\omega_{2b,b} = \omega_{b,0} - \Delta_b$, $\omega_{ab,a} = \omega_{b,0} - \Delta_{ab}$, $\omega_{ab,b} = \omega_{a,0} - \Delta_{ab}$, $\omega_{2a,b} = 2\omega_{a,0} - \omega_{b,0} - \Delta_a$ and $\omega_{2b,a} = 2\omega_{b,0} - \omega_{a,0} - \Delta_b$. These frequencies represent transitions from singly excited states to overtones, to the combination band, or otherwise forbidden three quantum transitions.

For the IR-PE experiment on vibrational systems, there are three general interfering Feynman diagrams that describe the propagation of coherences in Liouville space [3,37]. When extended to consider all six levels, there are 20 possible vibronic pathways that contribute to the vibrational part of the response function. These are represented as 20 different ladder diagrams in Fig. 2. Diagrams I(a–d) show the system oscillating at

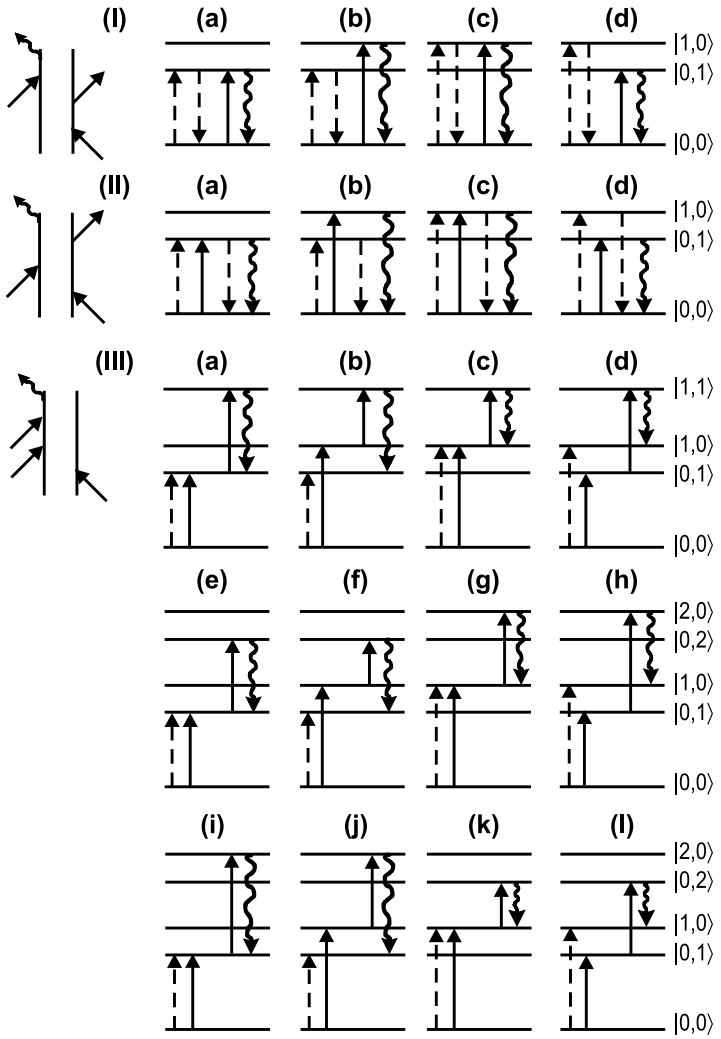

Fig. 2. The 20 different vibronic pathways resulting from three Feynman diagrams following the rotating wave approximation, which contribute to the vibronic part of the third-order response function. Diagrams I and II show correlations between one-quantum transitions in both the time periods. Ladder diagrams corresponding to Feynman diagram III, show correlations between the one-quantum and the two-quantum states.

either of the fundamental frequencies during both the coherence periods. Diagrams II(a–d) also concern themselves with dynamics in the one-quantum manifold except that the system is in an excited state population during τ_2. Diagrams III(a–l) show the system oscillating at one of the fundamental frequencies during τ_1, and oscillating in a coherence involving a two-quantum state during τ_3. Diagrams III(f, h–l) involve three quantum transitions for the third interaction, and would not exist in the harmonic approximation. These transitions become allowed because of the mixing of the harmonic oscillator eigenfunctions.

The response functions for each of the 20 pathways are calculated using a Bloch model with a phenomenological damping constant Γ_{ij}. The response function, $\mathbf{R}^{(3)}(\tau_1, \tau_2, \tau_3)$, can be Fourier transformed along the time coordinates τ_1 and τ_3

$$S(\Omega_1,\Omega_3)=\int_{-\infty}^{\infty}\mathrm{d}\tau_1\int_{-\infty}^{\infty}\mathrm{d}\tau_3\mathbf{R}^{(3)}(\tau_1,\tau_3)\times\exp(\mathrm{i}\Omega_1\tau_1)\exp(\mathrm{i}\Omega_3\tau_3)\qquad(12)$$

to yield a 2D spectrum. The spectrum displays the 2D data intuitively as a map of frequencies, Ω_1 and Ω_3, sampled by the system during each of the experimentally controlled time periods. In a 2D experiment, $\tau_2=0$, and is therefore neglected. For the Bloch model, the Fourier transformed PE signal can be written as:

$$\begin{aligned}S(\Omega_1,\Omega_3)=&\frac{2\mu_{a,0}^4}{[\mathrm{i}(\Omega_1+\omega_{a,0})+\Gamma_{a,0}][\mathrm{i}(\Omega_3-\omega_{a,0})+\Gamma_{a,0}]}+\frac{2\mu_{b,0}^4}{[\mathrm{i}(\Omega_1+\omega_{b,0})+\Gamma_{b,0}][\mathrm{i}(\Omega_3-\omega_{b,0})+\Gamma_{b,0}]}\\&+\frac{2\mu_{a,0}^2\mu_{b,0}^2}{[\mathrm{i}(\Omega_1+\omega_{a,0})+\Gamma_{a,0}][\mathrm{i}(\Omega_3-\omega_{b,0})+\Gamma_{b,0}]}+\frac{2\mu_{a,0}^2\mu_{b,0}^2}{[\mathrm{i}(\Omega_1+\omega_{b,0})+\Gamma_{b,0}][\mathrm{i}(\Omega_3-\omega_{a,0})+\Gamma_{a,0}]}\\&-\frac{\mu_{ab,a}\mu_{a,0}\left(\mu_{ab,a}\mu_{a,0}+\mu_{ab,b}\mu_{b,0}\right)}{[\mathrm{i}(\Omega_1+\omega_{a,0})+\Gamma_{a,0}][\mathrm{i}(\Omega_3-\omega_{b,0}+\mathrm{i}\Delta_{ab})+\Gamma_{ab,a}]}\\&-\frac{\mu_{ab,b}\mu_{b,0}\left(\mu_{ab,b}\mu_{b,0}+\mu_{ab,a}\mu_{a,0}\right)}{[\mathrm{i}(\Omega_1+\omega_{b,0})+\Gamma_{b,0}][\mathrm{i}(\Omega_3-\omega_{a,0}+\Delta_{ab})+\Gamma_{ab,b}]}\\&-\frac{\mu_{2a,a}\mu_{a,0}\left(\mu_{2a,a}\mu_{a,0}+\mu_{2a,b}\mu_{b,0}\right)}{[\mathrm{i}(\Omega_1+\omega_{a,0})+\Gamma_{a,0}][\mathrm{i}(\Omega_3-\omega_{a,0}+\Delta_a)+\Gamma_{2a,a}]}\\&-\frac{\mu_{2b,b}\mu_{b,0}\left(\mu_{2b,b}\mu_{b,0}+\mu_{2b,a}\mu_{a,0}\right)}{[\mathrm{i}(\Omega_1+\omega_{b,0})+\Gamma_{b,0}][\mathrm{i}(\Omega_3-\omega_{b,0}+\Delta_b)+\Gamma_{2b,b}]}\\&-\frac{\mu_{2b,a}\mu_{a,0}\left(\mu_{2b,a}\mu_{a,0}+\mu_{2b,b}\mu_{b,0}\right)}{[\mathrm{i}(\Omega_1+\omega_{a,0})+\Gamma_{a,0}][\mathrm{i}(\Omega_3-2\omega_{b,0}+\omega_{a,0}+\Delta_b)+\Gamma_{2b,a}]}\\&-\frac{\mu_{2a,b}\mu_{b,0}\left(\mu_{2a,b}\mu_{b,0}+\mu_{2a,a}\mu_{a,0}\right)}{[\mathrm{i}(\Omega_1+\omega_{b,0})+\Gamma_{b,0}][\mathrm{i}(\Omega_3-2\omega_{a,0}+\omega_{b,0}+\Delta_a)+\Gamma_{2a,b}]}.\end{aligned}\qquad(13)$$

Here μ_{ij} represents the transition dipole matrix element $\langle i|\hat{\mu}|j\rangle$, with $\hat{\mu}$ being the dipole operator. The first two terms on the right hand side of Eq. (13) arise from diagrams I(a,c) and II(a,c). The second two terms arise from I(b,d) and II(b,d). Similarly, diagrams III(a–l) give rise to terms 5–10 respectively.

Before discussing specific vibrational interactions giving rise to 2D spectra, first consider the form of Eq. (13) for a purely harmonic system. The absence of anharmonicity implies that $\Delta_a=\Delta_b=\Delta_{ab}=0$. For a linear transition dipole moment, the dipole matrix elements follow the harmonic approximation, $\mu_{n,n-1}=\sqrt{n}\mu_{1,0}$, such that $\mu_{2a,a}=\sqrt{2}\mu_{a,0}$, $\mu_{2b,b}=\sqrt{2}\mu_{b,0}$, $\mu_{ab,a}=\mu_{a,0}$, $\mu_{ab,b}=\mu_{b,0}$ and $\mu_{2b,a}=\mu_{2a,b}=0$. We also assume that the dephasing constants for a particular fundamental frequency are the same: $\Gamma_{2a,a}=\Gamma_{ab,a}=\Gamma_{a,0}$ and $\Gamma_{2b,b}=\Gamma_{ab,b}=\Gamma_{b,0}$. These constraints lead to destructive interferences that cause the nonlinear response to vanish. In this limit, Eq. (13) vanishes due to cancellations between the first four terms, which arise from purely one-quantum coherences, and the last six terms, which involve transitions into the two-quantum manifold. It becomes evident that in order to observe a 2D IR signal, one or more of the following conditions must be met: (1) ground state anharmonicity, (2) nonlinearity in the transition dipole moment, and (3) level-dependent dephasing dynamics. In the following section, it is shown that these conditions lead to distinct signatures in the 2D IR PE spectrum.

3. Vibrational interactions in 2D IR experiments

3.1. Anharmonicity in the ground state potential surface

Anharmonicity in the nuclear potential leads to frequency shifts between fundamental transitions and transitions to two-quantum manifold. These anharmonic splittings, described by Eq. (11), lead to shifts of the various resonances in Eq. (13), and thereby lead to the appearance of 10 peaks in the 2D spectrum. Thus anharmonicity of the system can be investigated by measuring peak splittings in the ω_3 dimension.

We demonstrate this effect using parameters that are used to reproduce the 2D IR PE spectrum of rhodium(I) dicarbonylacetylacetonate ($Rh(CO)_2$-$(C_5H_7O_2)$, or RDC) in hexane [27]. The fundamental transition frequencies, $\omega_{a,0}$ and $\omega_{b,0}$, taken from the absorption peaks of the symmetric and asymmetric CO stretches in the FTIR spectrum, are 2085 and 2014 cm^{-1} respectively. The values of the anharmonic splittings Δ_a, Δ_b, and Δ_{ab}, were taken to be 10.6, 12, and 25 cm^{-1}, respectively. These values correspond closely to what has been observed in transient pump–probe and PE experiments on this compound. From Eqs. (5a)–(5f), the anharmonic parameters for the nuclear potential are calculated to be $g_{aaa} = 32$ cm^{-1}, $g_{bbb} = 32$ cm^{-1}, and $g_{aab} = g_{abb} = 22$ cm^{-1}. The amplitudes of the 10 peaks are determined by the transition dipole moments, μ_{ij}. Here, the dipole moments have been expanded linearly in each of the vibrational coordinates. The matrix elements for each of the transitions are calculated using the harmonic oscillator eigenfunctions corrected to first order. This results in the following transition dipole moments scaling relationships: $\mu_{b,0} = \mu_{a,0}$; $\mu_{2a,a} = \mu_{2b,b} = 1.3\mu_{a,0}$; $\mu_{ab,a} = \mu_{ab,b} = 0.9\mu_{a,0}$; $\mu_{2a,b} = \mu_{2b,a} = -0.04\mu_{a,0}$; which vary modestly from the harmonic approximation: $\mu_{2a,a} = \sqrt{2}\mu_{a,0}$; $\mu_{ab,a} = \mu_{a,0}$; and $\mu_{2b,a} = 0$. All the dephasing constants, Γ_{ij}, are taken to be constant and equal to 1 cm^{-1}.

Incorporating all the values of the anharmonic splittings and the transition dipole moments given above in Eq. (13) results in an absolute value 2D IR PE spectrum shown in Fig. 3(a). Ten peaks are observed and they can be associated with each of the 20 vibronic pathways shown in Fig. 2. Table 1, labels each of the 10 peaks with their corresponding positions and the ladder diagrams that created them. All resonances in the Ω_1 dimension

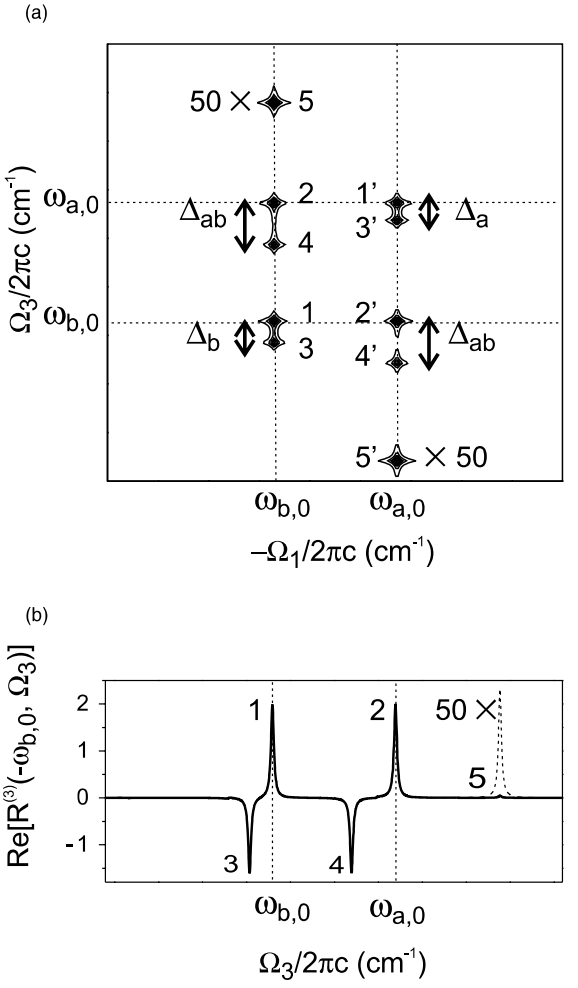

Fig. 3. (a) The absolute value 2D IR PE spectrum of two anharmonically coupled vibrations. The values in the nuclear potential are: $\omega_a^0 = 2101$ cm^{-1}, $\omega_b^0 = 2034$ cm^{-1}, $g_{aab} = g_{abb} = 22$ cm^{-1}, $g_{aaa} = 32$ cm^{-1}, $g_{bbb} = 32$ cm^{-1} resulting in $\Delta_a = 10.6$ cm^{-1}, $\Delta_b = 12$ cm^{-1} and $\Delta_{ab} = 25$ cm^{-1}. The dipole moment is expanded linearly in the vibrational coordinates with $\mu_a^{(1)} = \mu_b^{(1)} = 1$. The various transition dipole moments in terms of $\mu_{a,0}$ are: $\mu_{b,0} = \mu_{a,0}$, $\mu_{2a,a} = \mu_{2b,b} = 1.3\mu_{a,0}$, $\mu_{ab,a} = \mu_{ab,b} = 0.9\mu_{a0}$, $\mu_{2a,b} = \mu_{2b,a} = -0.04\mu_{a,0}$. All the dephasing constants, Γ are taken to be constant and equal to 1 cm^{-1}. (b) The real part of the spectrum showing a slice along $\Omega_1 = -\omega_{b,0}$ showing the relative signs of the coherences oscillating during τ_3.

Table 1
Positions of the various peaks for a system of two anharmonically coupled vibrational modes, v_a and v_b on a 2D IR PE spectrum as a function of Ω_1 and Ω_3 along with the corresponding ladder diagram from Fig. 2 giving rise to the resonances

Peaks	Position		Ladder diagram
	Ω_1	Ω_3	
1	$-\omega_{b,0}$	$\omega_{b,0}$	I(a), II(a)
2	$-\omega_{b,0}$	$\omega_{a,0}$	I(b), II(b)
3	$-\omega_{b,0}$	$\omega_{2b,b}$	III(e,f)
4	$-\omega_{b,0}$	$\omega_{ab,b}$	III(a,b)
5	$-\omega_{b,0}$	$\omega_{2a,b}$	III(i,j)
1′	$-\omega_{a,0}$	$\omega_{a,0}$	I(c), II(c)
2′	$-\omega_{a,0}$	$\omega_{b,0}$	I(d), II(d)
3′	$-\omega_{a,0}$	$\omega_{2a,a}$	III(g,h)
4′	$-\omega_{a,0}$	$\omega_{ab,a}$	III(c,d)
5′	$-\omega_{a,0}$	$\omega_{2b,a}$	III(k,l)

lie at one of the two fundamental frequencies, reflecting the two possible coherences excited during τ_1. (These two possibilities are distinguished by numbering the peaks with or without a prime.) The features on the diagonal axis and the cross-peaks each consist of a pair of closely spaced peaks split along Ω_3, corresponding to coherences amongst adjacent levels. For example, peaks 1 and 3 represent the system evolving during τ_3 in $|01\rangle\langle 00|$ and $|02\rangle\langle 01|$ coherences respectively. These frequencies are split by Δ_b. Peaks 2 and 4 represent the system evolving in $|10\rangle\langle 00|$ and $|11\rangle\langle 01|$ coherences respectively during τ_3. These frequencies are split by Δ_{ab}. Similar arguments can be made for peaks 1′–4′.

In addition to these eight peaks, the presence of the anharmonicity leads to two otherwise forbidden transitions at 5 and 5′. These peaks involve three-quantum transitions during the final field interaction involving changes of quantum number for both states subject to $(\Delta n + \Delta k) = \pm 1$. The amplitude of peak 5 has to be multiplied by a factor of 50 for its contours to be at the same order of magnitude as the other peaks. Harmonically forbidden transitions also contribute to the amplitude of peaks 3 and 3′, through level diagrams, III(f) and III(h). However the contribution of these diagrams is just 3% of the total amplitude of these peaks.

For a system of two anharmonically coupled vibrations, the 10 peaks lie on specific diagonal or anti-diagonal axes. The diagonal axis is defined as

$$-\Omega_1 = \Omega_3 \tag{14}$$

and anti-diagonal axes are defined as

$$-\Omega_1 + \Omega_3 = \text{ constant}. \tag{15}$$

Two peaks along the diagonal axis (1 and 1′) represent the individual fundamental vibrations of the system, which arise from the coherences between the ground and one-quantum states during τ_1 and τ_3. The remaining eight peaks lie along anti-diagonal axis. The cross-peaks (peaks 2 and 2′) lie on the anti-diagonal axis defined as: $-\Omega_1 + \Omega_3 = \omega_{a,0} + \omega_{b,0}$. These peaks result from the system oscillating in coherences involving the ground state and different one-quantum manifold states during τ_1 and τ_3. Peaks 4 and 4′ arise from the system oscillating at one of the fundamental frequencies during τ_1 and in a coherence involving the $|1,1\rangle$ state during τ_3. These peaks also lie along the anti-diagonal, $-\Omega_1 + \Omega_3 = \omega_{a,0} + \omega_{b,0} - \Delta_{ab}$, parallel to the cross-peaks, and separated by the anharmonic splitting, Δ_{ab}. Peaks 3 and 5′ also lie on an anti-diagonal defined by $-\Omega_1 + \Omega_3 = 2\omega_{b,0} - \Delta_b$. Similarly peaks 5 and 3′ lie along $-\Omega_1 + \Omega_3 = 2\omega_{a,0} - \Delta_a$. These rules can aid in describing congested multi-level spectra with arbitrary anharmonic splittings: Δ_a, Δ_b and Δ_{ab}.

To illustrate the relative signs of the five peaks, Fig. 3b shows a slice of the real part of the 2D spectrum along Ω_3, for $\Omega_1 = -\omega_{b,0}$. Peaks 1 and 2, which arise only from transitions between the ground and one-quantum manifold, are of opposite sign from peaks 3 and 4, which involve transitions to the two-quantum states. Absence of the anharmonic splitting ($\Delta_b = 0$) would lead to the resonances for peaks 1 and 3 at the same value of Ω_3, and destructive interference between these contributions would lead to zero signal along the diagonal axis. A similar argument can be made for the cross-peaks 2 and 4, which are separated by Δ_{ab}. The peak splitting between peaks 2 and 4 would disappear in the limit of zero off-diagonal anharmonicity ($g_{aab} = g_{abb} = 0$).

Fig. 3 demonstrates that the presence of ground state anharmonicity results in 10 peaks in the 2D

spectrum described by energy differences Δ_a, Δ_b and Δ_{ab}, and unequal amplitudes of the peak pairs 1, 3 and 2, 4. The position of the various peaks allows us to map out the six-level energy structure shown in Fig. 1 in a very intuitive fashion. The experimentally observed energy splittings, Δ_a, Δ_b and Δ_{ab} can be further related to the diagonal and off-diagonal anharmonic coupling parameters, g_{ijk}, if we take all off-diagonal elements to be equal, i.e. $g_{aab} = g_{abb}$.

Once anharmonicities are known, it remains to determine what the microscopic origin of coupling is. This is of particular interest for extracting information on molecular structure. In particular, if anharmonicity arises from through-space electrostatic interactions that can be modeled as dipole–dipole coupling [38], then 2D vibrational spectra can be used to directly measure distances between interacting dipoles, and polarization selective measurements can be used to extract their orientation. The structural information for the 2D IR PE would be transient, with an effective time resolution dictated by the homogeneous line widths of the system.

3.2. Nonlinear transition dipole moment

Generally, the dipole moment of a molecule, expressed as a function of its vibrational coordinates can be expanded in a power series about the equilibrium configuration Q_0 [39]

$$\tilde{\mu} = \tilde{\mu}(Q_0) + \sum_i \left(\frac{\partial\tilde{\mu}}{\partial Q_i}\right)_{Q_0} Q_i + \frac{1}{2}\sum_{i,j}\left(\frac{\partial\tilde{\mu}}{\partial Q_i\partial Q_j}\right)_{Q_0} Q_iQ_j + \frac{1}{6}\sum_{i,j,k}\left(\frac{\partial\tilde{\mu}}{\partial Q_i\partial Q_j\partial Q_k}\right)_{Q_0} Q_iQ_jQ_k + \cdots \quad (16a)$$

$$\tilde{\mu} = \mu^{(0)} + \sum_i \mu_i^{(1)} Q_i + \frac{1}{2}\sum_{i,j}\mu_{ij}^{(2)} Q_iQ_j + \frac{1}{6}\sum_{i,j,k}\mu_{ijk}^{(3)} Q_iQ_jQ_k + \cdots. \quad (16b)$$

The magnitude and sign of the expansion coefficients $\mu^{(1)}$ and $\mu^{(2)}$ represent the tangent and curvature of the dipole moment at equilibrium. When molecules interact with electromagnetic radiation through the transition dipole moment, which represents the change of charge distribution through the field-induced displacement of the normal coordinates. The selection rule for linear spectroscopy in the dipole approximation considers only the terms linear in the vibrational coordinates. Thus, for a particular mode, i to be IR active, $\mu_i^{(1)} \neq 0$, and the selection rule of $\Delta n = \pm 1$ is obtained. As illustrated in Eq. (13), using the dipole approximation in a harmonic system leads to a zero 2D signal. In addition to the peak splitting phenomenon observed with vibrational anharmonicity, the destructive interference between quantum pathways can also be broken by considering the nonlinear dependence of the transition dipole moment on the vibrational coordinates, i.e. electrical anharmonicity. The effects of electrical anharmonicity have been studied experimentally [40] by observing the intensities of fundamental and overtone bands as well as theoretically using ab initio methods to calculate dipole moment surfaces [41, 42]. The results of Fair et al. indicate that the electrical anharmonicity causes the transition dipole moment vector of the OH stretch to rotate counter clockwise from the OH bond by almost 20° going from v_{OH} to $4v_{OH}$. The 2D dipole moment surface calculated for the isolated CH chromophore in $CHCl_3$ using ab initio methods by Lin et al. show that values of $\mu^{(2)}$ range from 20–200% of $\mu^{(1)}$.

To investigate the nonlinear dipole, let us first consider a harmonic system of two uncoupled normal modes with fundamental frequencies $\omega_{a,0}$ and $\omega_{b,0}$. Following Eq. (16), the dipole moment for this system is expanded in the vibrational coordinates (Q_a and Q_b), and the nonlinear expansion terms are considered to be invariant to the interchange of indices. For the harmonic system, the expansion must be continued to third order, since second-order dipole matrix elements ($\Delta n + \Delta k = 0, \pm 2$), do not contribute to the one-quantum transitions observed in this experiment ($\Delta n + \Delta k = \pm 1$). Setting $\mu_{ijk}^{(3)} = 0.08\mu_i^{(1)}$, the various transition dipole moments are calculated to be $\mu_{b,0} = \mu_{a,0} = 1$; $\mu_{2a,a} = \mu_{2b,b} = 1.5\mu_{a,0}$; $\mu_{ab,a} = \mu_{ab,b} = 1.07\mu_{a,0}$;

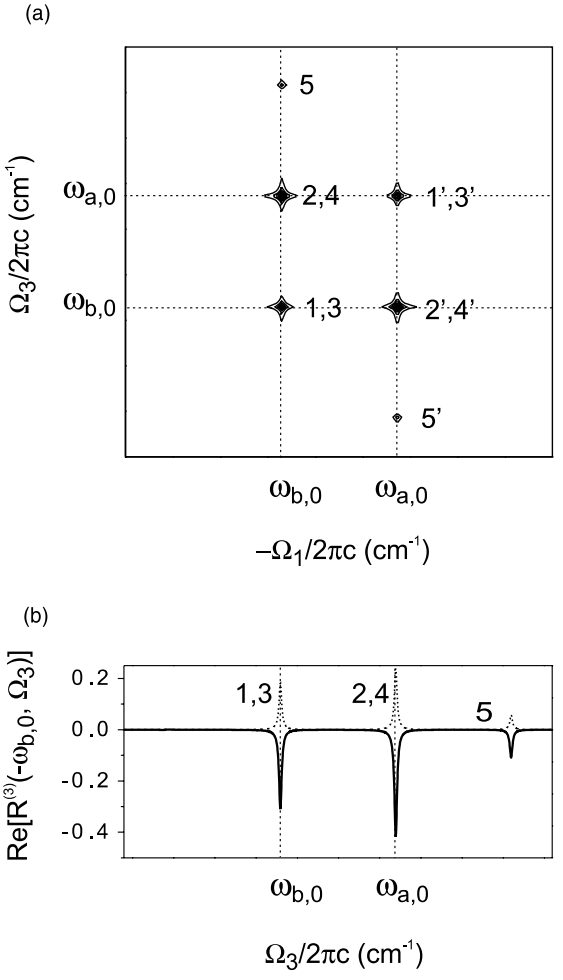

Fig. 4. Nonlinear dependence of the transition dipole moment on the vibrational coordinates. (a) The absolute value 2D IR PE spectrum for two harmonic modes where the dipole moment has been expanded to third-order in the vibrational coordinates. In this simulation the value of $\mu_i^{(1)} = 1$ and all $\mu_{ijk}^{(3)} = 0.08\mu_i^{(1)}$. The values of the dipole parameters are: $\mu_{b,0} = \mu_{a,0} = 1$, $\mu_{2a,a} = \mu_{2b,b} = 1.5\mu_{a,0}$, $\mu_{ab,a} = \mu_{ab,b} = 1.07\mu_{a0}$, $\mu_{2b,a} = \mu_{2a,b} = 0.05\mu_{a,0}$ (b) The real part of the spectrum showing a slice along $\Omega_1 = -\omega_{b,0}$ for the absolute value 2D spectrum in (a). The straight and dotted lines show the 2D echo signal for $\mu_{ijk}^{(3)} = 0.08\mu_i^{(1)}$ and for $\mu_{ijk}^{(3)} = -0.08\mu_i^{(1)}$ respectively.

$\mu_{2b,a} = \mu_{2a,b} = 0.05\mu_{a,0}$. Expansion of the dipole moment to third-order in the vibrational coordinates makes harmonically forbidden transitions such as, $|1,0\rangle \rightarrow |0,2\rangle$ possible. The 2D IR PE signal can be calculated using these dipole matrix elements, together with the previous fundamental frequencies and damping constants, and is plotted in Fig. 4(a). Note that in the absence of any anharmonicity in the ground state potential, $\Delta_a = \Delta_b = \Delta_{ab} = 0$.

The 2D spectrum in Fig. 4(a) shows two features along the diagonal and two-cross-peaks along the anti-diagonal. Due to the lack of anharmonicity, coherences involving adjacent vibrational levels oscillate at the same frequency. This results in peaks 3 and 4 being at the same position as peaks 1 and 2 respectively. Peak 5(5′) results from the system evolving in the $|20\rangle\langle 01|$ ($|02\rangle\langle 10|$) coherence during τ_3. Relative to Fig. 3a, it is shifted in position by $\Delta_a(\Delta_b)$, as there is no anharmonicity present in this simulation. Peaks 1 and 2 are of unequal amplitude and the magnitude of peak 5 is one-third that of peak 1. This is seen more clearly in the real part of the spectrum plotted in Fig. 4(b). The solid line in Fig. 4(b) shows a slice of the real part of the 2D spectrum along Ω_3 for $\Omega_1 = -\omega_{b0}$ showing that all peaks have the same sign. Changing the sign of $\mu_{ijk}^{(3)}$ to negative changes the sign of the peaks, although this results in a smaller overall amplitude.

When vibrational anharmonicity is included with the nonlinear dipole expansion, both effects can be observed and separated in 2D spectra. As in Fig. 3a, 10 peaks are observed at positions dictated by the anharmonic parameters. The inclusion of the nonlinear transition dipole reveals itself as a difference in the amplitude of different peak pairs that interfere in the harmonic limit. In general, peaks 1, 2 and 5 will have opposite sign from peaks 3 and 4. The difference in amplitude between peak pair 1 and 3 and peak pair 2 and 4 reflects the magnitude of the correction to harmonic scaling from electrical anharmonicity.

3.3. Quantum number dependence of dephasing

Imperfect cancellation between destructively interfering quantum pathways can also occur if the dynamics for the interfering levels are different. This third selection rule implies that conditions leading to $\Gamma_{a,0} \neq \Gamma_{2a,a}$ and $\Gamma_{a,0} \neq \Gamma_{ab,a}$, i.e. quantum-number-dependent dephasing, will lead to a 2D signal. These types of dynamics will arise from

coupling either between the system states, or between the system and bath.

Vibrational relaxation of a multi-level system can occur through pure dephasing, population relaxation, coherence transfer and population transfer. The Redfield equations of the density matrix account for these relaxation pathways through a superoperator $\Gamma_{iji'j'}$ which couples the various elements of the density matrix [43]. The secular approximation, which is used in the Bloch equations, considers only the Γ_{ijij} elements of the relaxation operator. The effects of coherence transfer and population transfer are ignored in this approximation resulting in the familiar representation of the decay rate:

$$\Gamma_{ij} = \tfrac{1}{2}\left(\Gamma_{ii} + \Gamma_{jj}\right) + \gamma_{ij}, \tag{17}$$

where Γ_{ii} and Γ_{jj} are the population decay rates out of states i and j and γ_{ij} is the pure dephasing rate.

To illustrate possible quantum number scaling relationships for vibrational dephasing, population and phase relaxation of our two coordinate system is considered using a model of a harmonic system coupled to a quantum mechanical bath consisting of linearly coupled harmonic oscillators [37,44]. This model has been used to study the nonlinear signals obtained in third- and fifth-order Raman scattering experiments [16,45–47], relaxation of product species following photolysis [48] and two-pulse PEs for harmonic as well as anharmonic systems [37,49]. Population relaxation term is obtained by considering linear coupling of the harmonic system oscillators to each of the bath oscillators and the pure dephasing rate arises from a quadratic coupling between system and bath. This is a direct approach to obtain level-dependent dephasing dynamics.

For two harmonic oscillators linearly coupled to a quantum bath, the downward rate of population relaxation from a state $|i\rangle$ with quantum numbers nk is given by:

$$\Gamma_{ii} \propto |\langle n-1, k-1|Q_a + Q_b|n,k\rangle|^2 \propto n + k. \tag{18}$$

The downward rate of population relaxation scales with the quantum number of the initial state. Using the above equation along with Eq. (17) and assuming that $\Gamma_{a,0} = \Gamma_{b,0}$, it can be shown that $\Gamma_{2a,a} = \Gamma_{2b,b} = \Gamma_{ab,a} = \Gamma_{ab,b} = 3\Gamma_{a,0}$. Note that pure dephasing (γ_{ij}) has been neglected, and the dephasing rates are given exclusively by population relaxation.

In the case of population relaxation, such linear coupling to the bath can be related to a description of the bath friction on the system coordinate. In this model, the system–bath interaction potential is expanded as a Taylor series in the system coordinate, where a bath operator multiplies each expansion term. The bath operators can be expressed as force–force autocorrelation functions whose power spectrum describes the friction on the vibrational coordinate. In Eq. (18) the bath operators have not been accounted for and population relaxation has been expressed only in the system coordinates. The reader is referred to a paper by Oxtoby and Rice [44] for a thorough treatment of this model where a general relationship is derived between population relaxation, pure dephasing and the homogeneously broadened Raman line width.

Neglecting population relaxation, the pure dephasing rate, γ_{ij} for states $|i\rangle$ and $|j\rangle$ with respective quantum numbers nk and $n'k'$ can be obtained by the quadratic coupling of the system to the bath. It is written below only in terms of the system coordinates:

$$\begin{aligned}\gamma_{ij} &\propto \left|\langle n,k|Q_a^2 + Q_b^2|n,k\rangle - \langle n',k'|Q_a^2 + Q_b^2|n',k'\rangle\right|^2 \\ &\propto 4\left(n - n' + k - k'\right)^2.\end{aligned} \tag{19}$$

For our six-level system, the pure dephasing rate for coherent superpositions of one- and two-quantum states will be identical to those coherences between the one-quantum and the ground states. To this approximation, all γ_{ij} will be the same.

Pure dephasing is known to occur through nonlinear coupling of the system to the bath as shown above and through the anharmonicity present in the isolated molecular vibration [50, 51]. The effect of anharmonicity in the vibrational mode on the pure dephasing has been studied using the generalized Langevin equation

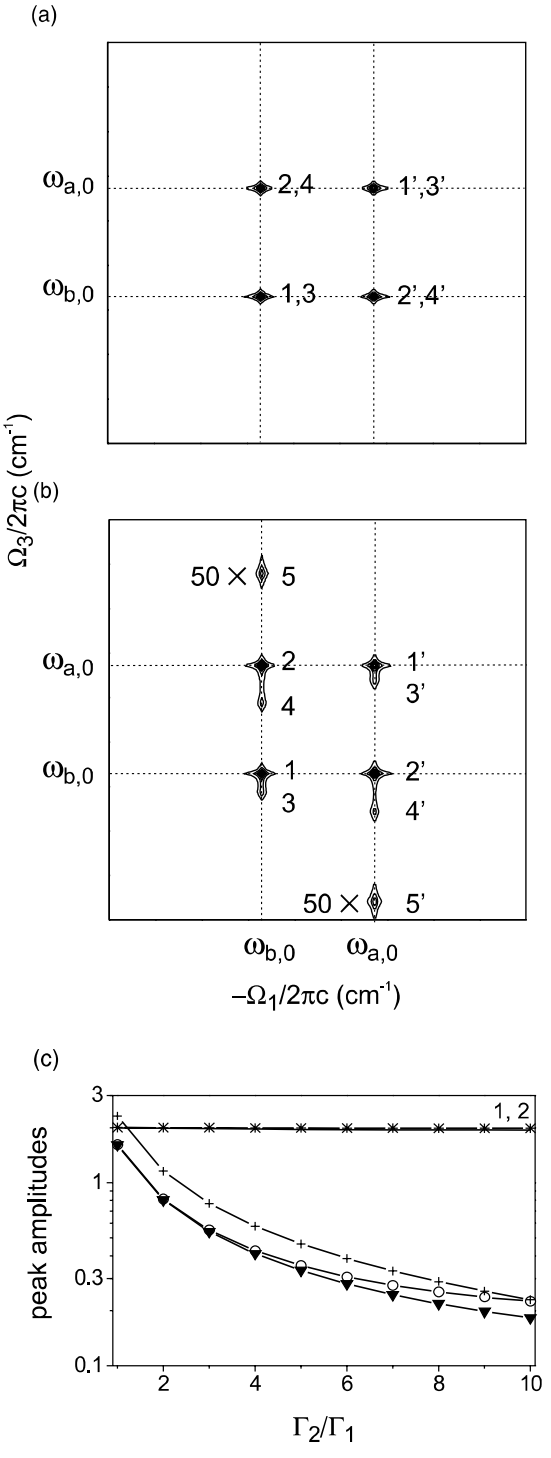

Fig. 5. Level-dependent population relaxation. (a) The absolute value 2D IR PE spectrum for a harmonic oscillator coupled linearly to a bath. The values for the dephasing constants are: $\Gamma_{a,0} = \Gamma_{b,0} = 1$ cm^{-1} and $\Gamma_{2a,a} = \Gamma_{2b,b} = \Gamma_{ab,a} = \Gamma_{ab,b} = 3\Gamma_{a,0}$. The dipole moments follow harmonic scaling. (b) Anharmonically coupled oscillators coupled linearly to a bath of harmonic oscillators. The values for the transition dipole moments and the anharmonicity parameters are the same as those in Fig. 3(a). The dephasing constants are defined as in (a). (c) Dependence of peak heights as a function of Γ_2/Γ_1. Γ_2 represents $\Gamma_{2b,b}$, $\Gamma_{ab,b}$ and $\Gamma_{2a,b}$, and Γ_1 represents $\Gamma_{b,0}$. The symbols ✳, +, ○ and ▼ represent peaks 1–2, 3, 4 and 5 respectively.

[52,53] and a hydrodynamic model for a cubic anharmonic oscillator in a quantum and classical bath [54]. Molecular dynamics simulations have also been performed for an anharmonic oscillator in a Lennard-Jones bath [55,56]. These studies emphasize the importance of the vibrational anharmonicity present in the system when the spectral density of the bath at the vibrational frequency is minimal. In this paper, we account for the pure dephasing only through the nonlinear coupling to the bath as our two-coordinate system is considered to be harmonic. Since all the γ_{ij} are identical in this model, we have not accounted for the pure dephasing to demonstrate level-dependent dephasing dynamics.

We consider the effect of level-dependent dephasing dynamics in 2D spectra by calculating the case of vibrational dephasing dominated by lifetime broadening, $\gamma_{ij} = 0$. We use two harmonic oscillators with fundamental frequencies $\omega_{a,0}$ and $\omega_{b,0}$, $\Delta_a = \Delta_b = \Delta_{ab} = 0$, and harmonic scaling of the transition dipole moment. The dephasing rates reflecting only the population relaxation are $\Gamma_{a,0} = \Gamma_{b,0} = 1$ cm^{-1}, and $\Gamma_{2a,a} = \Gamma_{2b,b} = \Gamma_{ab,a} = \Gamma_{ab,b} = 3$ cm^{-1}. The level-dependent dephasing parameters result in the imperfect cancellation of response functions involving the one-quantum and two-quantum states giving rise to a 2D IR PE signal. The absolute value 2D spectrum is plotted in Fig. 5(a). Four peaks are observed, two diagonal and two cross-peaks. These appear in the same position at peaks 1–4 in Fig. 4a, although now the shape of the peaks is elongated along the Ω_1 direction.

Level-dependent dephasing reveals itself in the asymmetric shape of the peaks in the 2D IR PE spectrum. Since the dephasing is faster during τ_3, it is expected that peaks would be broadened in the Ω_3 direction, but the opposite is observed. This counter-intuitive result occurs because of the different line shapes associated with the destructively interfering pathways contributing to these peaks. The 2D line shapes arising from coherences between the one-quantum manifold and ground state during τ_3 have a symmetric diamond shape, since they dephase at the same rate during both the time periods. The 2D line shapes arising from coherences between the one and two-quantum manifold during τ_3 are broadened along the Ω_3 direction, as they dephase three times as fast during the second time period. The interference between these contributions lead to the line shape observed in Fig. 5a.

The interfering contributions are resolved in a system where anharmonicity in the ground state potential is included with lifetime broadening. Fig. 5b shows the characteristic asymmetric broadening of peaks 3 and 4 along the Ω_3 direction. A comparison of Fig. 5b with Fig. 3a also shows that the change in the dephasing parameters results in a lower amplitude of peaks 3–5, while peaks 1 and 2 remain unaffected. Thus level-dependent dephasing affects the shape and amplitude of the 2D line shape.

Dephasing and population relaxation measurements of fundamental and overtone transitions have resulted in various quantum number scaling relationships for the relaxation rate [48,57]. Fig. 5c plots the effects of arbitrary quantum number dependent dephasing of $\Gamma_{2b,b}$, $\Gamma_{ab,b}$ and $\Gamma_{2a,b}$ relative to $\Gamma_{b,0}$. The amplitude of all peaks are plotted for the ratio of the dephasing rates, Γ_2/Γ_1. The heights of peaks 3–5 drop rapidly, reflecting the increased dephasing rates along Ω_3, while the heights of peaks 1 and 2 are roughly constant.

The effect of anharmonicity on the level-dependent dephasing has been ignored here. Vibrational relaxation of an anharmonic potential can be modeled using a vibrational master equation approach to solve for the population relaxation accounting for both the upward and downward population relaxation in a quantum mechanical bath [48]. Alternatively, Redfield relaxation theory would allow population and coherence transfer to be addressed along with population relaxation and pure dephasing [58]. Pure dephasing has also been neglected, since quantum number dependent dynamics are not expected for a harmonic system coupled quadratically to a quantum bath. This result agrees with that obtained from Redfield theory for a 1D harmonic oscillator coupled to a thermal bath at zero temperature [58]. However, once anharmonicity is included the pure dephasing rate will become quantum-number dependent [52, 59].

4. Discussion and conclusions

We have considered three interaction mechanisms between vibrational coordinates, which can be observed through distinct signatures in the 2D IR PE spectrum. These interactions may be considered a set of selection (or propensity) rules that lead to a nonlinear optical response from the system. These include any interactions that lead to breaking of the purely harmonic behavior for which the 2D signal vanishes.

In practice, a distinct separation between these vibrational nonlinearities will not always be observed. Indeed, vibrational anharmonicity can influence all of them. Anharmonicity of the system coordinates leads to splitting of diagonal and cross-peaks in such a spectrum, and influences their amplitudes through the nonlinearity of the transition dipole. Anharmonicity involving the system or bath coordinates can lead to relaxation behavior that is quantum-number dependent, which also effects line shapes and amplitude.

The 2D IR PE spectrum allows the simultaneous influence of these effects to be observed. For the weak damping case ($\Gamma \ll \Delta$) described here, each of these effects can be separated and quantified in the absolute value spectrum. This is illustrated in Fig. 6a, which demonstrates the simultaneous effects of anharmonicity in the ground state potential, nonlinear dependence of the transition dipole moment on the vibrational coordinates, and level-dependent dephasing. We have

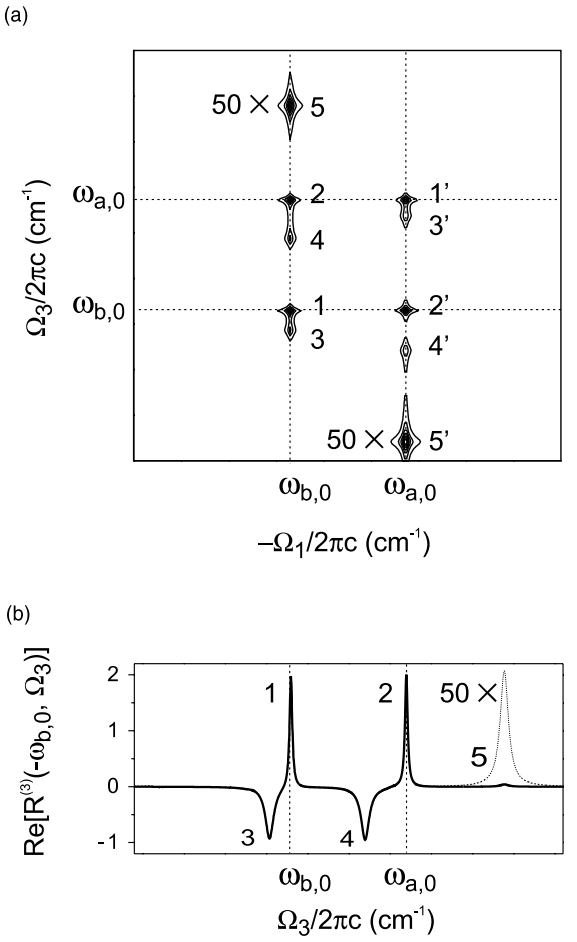

Fig. 6. (a) Combined effects of the anharmonicity of the ground state potential, expansion of the transition dipole moment in a nonlinear fashion on the coordinates and the quantum number dependence of the lifetime. The values of the anharmonicity parameters are those used in Fig. 3. The values of the transition dipole moments used to calculate Fig. 6 are: $\mu_i^{(1)} = 1$, $\mu_{ij}^{(2)} = 0.8\mu_i^{(1)}$ and $\mu_{ijk}^{(3)} = 0.08\mu_i^{(1)}$. This leads to: $\mu_{b,0} = \mu_{a,0}$, $\mu_{2a,a} = \mu_{2b,b} = 1.7\mu_{a,0}$, $\mu_{ab,a} = \mu_{ab,b} = 1.2\mu_{a0}$, $\mu_{2b,a} = -0.09\mu_{a,0}$ and $\mu_{2a,b} = -0.08\mu_{a,0}$. (b) The real part of the spectrum showing a slice along $\Omega_1 = -\omega_{b,0}$ with sensitivity to the relative signs of the coherences oscillating during τ_3.

used the parameters from previous examples, along with nonlinear dipole terms up to third order. The vibrational anharmonicity is measured through the energy splittings Δ_a, Δ_s and Δ_{ab}. The nonlinear dependence of the transition dipole moment on the vibrational coordinates results in unequal amplitudes of the diagonal (1,3) or cross-peak (2,4) pairs. The change in amplitude of peaks 3 and 4 is also due to the inclusion of quantum-number-dependent vibrational relaxation, which affects the amplitude of the resonances, along with elongation of two-quantum resonances in the Ω_3 dimension. A slice of the real part of the 2D spectrum at $\Omega_1 = -\omega_{b0}$ is shown in Fig. 6b. Again of the five peaks seen, peaks 3 and 4 have opposite sign than the rest, and their amplitudes differ from peaks 1 and 2. Also, the broader line width of peaks 3–5 reflect the quantum-number-dependent population relaxation.

The simulations presented here were chosen to mirror the anharmonicities and damping observed for RDC in hexane. Here the anharmonic splittings are much larger than the homogeneous dephasing width ($\Delta \gg \Gamma$), and homogeneous line broadening is a reasonable description of the dephasing dynamics. In other condensed phase systems, it should be expected that additional considerations will make a separation of the three vibrational nonlinearities more challenging. As observed in 2D IR spectroscopy of amide I vibrations, a more common situation may be case where homogeneous relaxation dynamics are relatively fast, and $\Delta \approx \Gamma$. For this limit, the absolute value spectrum is less useful since distinct anharmonic splittings and peak height variations will not be as clear. On the other hand, the real part of the spectrum will be more sensitive to the nature of the interfering contributions to the 2D spectrum. It is expected that the complex 2D line shape and spectrum will carry the same level of information presented here, by virtue of being sensitive both to amplitude and phase of the multiple coherent pathways.

Other structural and dynamic effects need to be considered in the modeling of the 2D IR PE spectrum. For a multi-level system such as this, the effects of population feeding and cross-relaxation should be considered using a master equation approach. This effect may give rise to additional resonances. For example, we could expect peaks at Ω_1, $\Omega_3 = -\omega_{a,0}$, $\omega_{2b,b}$ if population transfer occurs between levels $|a,0\rangle \rightarrow |0,b\rangle$ during τ_1 which results in the system evolving in the $\omega_{2b,b}$ coherence during τ_3.

The effects of inhomogeneous broadening have not been discussed in this simulation, although the signatures are understood [24,60,61]. Static inhomogeneous broadening or long time scale dephasing processes are observed on the diagonal peaks as elongation or ellipticity along the diagonal frequency axis. Inhomogeneous 2D line shapes need to be further described for a coupled multi-level system, with particular attention to the interference effects in the fast dephasing limit and the possibility of correlations between the inhomogeneous distributions of the coupled vibrations.

In addition to the isotropic treatment of vibrational coupling and relaxation presented here, orientational structural factors and dynamics must be included in a proper description of the 2D vibrational spectrum. As described in Eq. (9), the reorientational contribution to the response function is a fourth-rank tensor that carries the information on the relative orientation of the dipoles associated with the coupled vibrations and the reorientational dynamics of the individual vibrational states. Thus, the orientational response R^{or} will influence the relative amplitude of each of the vibronic Feynman diagrams by taking the order of interactions with particular dipoles into account. Also, the reorientational dynamics must be considered for each state, and could potentially influence the quantum-number dependence of dephasing. Measuring 2D spectra for different tensor elements can separate the influence of these orientational variables.

What is evident from the simulations of two anharmonically coupled oscillators is that a thorough analysis of 2D IR spectra can reveal a wealth of information regarding the strength and time course of vibrational interactions. We have shown that anharmonicity in the ground state potential, nonlinear dependence of the transition dipole moment on its vibrational coordinates and the quantum-number dependent dephasing are revealed in the positions, amplitudes and shape of the various peaks in the spectrum. If anharmonic coupling strengths and the dipole moment expansion coefficients can be related to physically relevant structural parameters, as in the case of dipole–dipole coupling, 2D IR PE spectroscopy can be used as a tool in determining transient molecular structure and its evolution.

Acknowledgements

We thank Dr. Oleg Golonzka for suggesting this investigation and for many subsequent discussions. This work was supported by the Office of Basic Energy Sciences, US Department of Energy (DE-FG02-99ER14988), the donors to the ACS-Petroleum Research Fund, and an award by the Research Corporation.

References

[1] D. Zimdars, A. Tokmakoff, S. Chen, S.R. Greenfield, M.D. Fayer, Phys. Rev. Lett. 70 (1993) 2718.
[2] A. Tokmakoff, D. Zimdars, R.S. Urdahl, R.S. Francis, A.S. Kwok, M.D. Fayer, J. Phys. Chem. 99 (1995) 13310.
[3] K.D. Rector, A.S. Kwok, C. Ferrante, A. Tokmakoff, C.W. Rella, M.D. Fayer, J. Chem. Phys. 106 (1997) 10027.
[4] P. Hamm, M. Lim, R.M. Hochstrasser, Phys. Rev. Lett. 81 (1998) 5326.
[5] R.F. Loring, S. Mukamel, J. Chem. Phys. 83 (1985) 2116.
[6] M. Berg, D.A. Vanden Bout, Acc. Chem. Res. 30 (1997) 65.
[7] S. Woutersen, U. Emmerichs, H.J. Bakker, Science 278 (1997) 658.
[8] P. Hamm, M. Lim, R.M. Hochstrasser, J. Phys. Chem. B 102 (1998) 6123.
[9] L.K. Iwaki, D.D. Dlott, J. Phys. Chem. A 104 (2000) 9101.
[10] R.R. Ernst, G. Bodenhausen, A. Wokaun, Principles of Nuclear Magnetic Resonance in One and Two Dimensions, Oxford University Press, Oxford, 1987.
[11] M. Cho, in: Y.F.a.S.H. Lin (Ed.), Advances in Multi-Photon Processes and Spectroscopy, vol. 12, World Scientific, Singapore, 1998, p. 1.
[12] S. Mukamel, Ann. Rev. Phys. Chem. 51 (2000) 691.
[13] S. Mukamel, A. Piryatinski, V. Chernyak, Acc. Chem. Res. 32 (1999) 145.
[14] Y. Tanimura, S. Mukamel, J. Chem. Phys. 99 (1993) 9496.
[15] A. Tokmakoff, M.J. Lang, D.S. Larsen, G.R. Fleming, V. Chernyak, S. Mukamel, Phys. Rev. Lett. 79 (1997) 2702.
[16] T. Steffen, J.T. Fourkas, K. Duppen, J. Chem. Phys. 105 (1996) 7364.
[17] K. Okumura, Y. Tanimura, J. Chem. Phys. 107 (1997) 2267.
[18] K. Okumura, A. Tokmakoff, Y. Tanimura, J. Chem. Phys. 111 (1999) 492.
[19] D.A. Blank, L.J. Kaufman, G.R. Fleming, J. Chem. Phys. 113 (2000) 771.

[20] V. Astinov, K.J. Kubarych, C.J. Milne, R.J.D. Miller, Chem. Phys. Lett. 327 (2000) 334.
[21] O. Golonzka, N. Demirdöven, M. Khalil, A. Tokmakoff, J. Chem. Phys. 113 (2000) 9893.
[22] P. Hamm, M. Lim, W.F. DeGrado, R.M. Hochstrasser, Proc. Nat. Acad. Sci. USA 96 (1999) 2036.
[23] P. Hamm, M. Lim, W.F. DeGrado, R.M. Hochstrasser, J. Chem. Phys. 112 (2000) 1907.
[24] M.C. Asplund, M.T. Zanni, R.M. Hochstrasser, Proc. Nat. Acad. Sci. USA 97 (2000) 8219.
[25] K.A. Merchant, D.E. Thompson, M.D. Fayer, Phys. Rev. Lett., submitted for publication.
[26] W. Zhao, J.C. Wright, Phys. Rev. Lett. 83 (1999) 1950.
[27] O. Golonzka, M. Khalil, N. Demirdoven, A. Tokmakoff, Phys. Rev. Lett., in press (2001).
[28] W.M. Zhang, V. Chernyak, S. Mukamel, J. Chem. Phys. 110 (1999) 5011.
[29] A. Piryatinski, S. Tretiak, V. Chernyak, S. Mukamel, J. Raman Spectrosc. 31 (2000) 125.
[30] C. Cohen-Tannoudji, B. Diu, F. Lalöe, Quantum Mechanics, Wiley–Interscience, Paris, 1977.
[31] B. Darling, D.M. Dennison, Phys. Rev. 57 (1940) 128.
[32] L.G. Bonner, Phys. Rev. 46 (1934) 458.
[33] S. Mukamel, Principles of Nonlinear Optical Spectroscopy, Oxford University Press, New York, 1995.
[34] S.M. Gallagher, A.W. Albrecht, J.D. Hybl, B.L. Landin, B. Rajaram, D.M. Jonas, J. Opt. Soc. Am. B 15 (1998) 2338.
[35] J.D. Hybl, A.W. Albrecht, S.M. Gallager-Faeder, D.M. Jonas, Chem. Phys. Lett. 297 (1998) 307.
[36] O. Golonzka, A. Tokmakoff, J. Chem. Phys., in preparation.
[37] J.T. Fourkas, H. Kawashima, K.A. Nelson, J. Chem. Phys. 103 (1995) 4393.
[38] M. Cho, Phys. Rev. A 61 (2000) 023406.
[39] G.H. Herzberg, Infrared and Raman Spectra of Polyatomic Molecules, Krieger, Malabar, FL, 1991.
[40] J.R. Fair, O. Votava, D.J. Nesbitt, J. Chem. Phys. 108 (1998) 72.
[41] H. Lin, L. Yuan, S. He, X. Wang, Q. Zhu, J. Chem. Phys. 112 (2000) 7484.
[42] K.K. Lehmann, A.M. Smith, J. Chem. Phys. 93 (1990) 6140.
[43] A.G. Redfield, Adv. Mag. Res. 1 (1965) 1.
[44] D.W. Oxtoby, S.A. Rice, Chem. Phys. Lett. 42 (1976) 1.
[45] T. Steffen, K. Duppen, Chem. Phys. 233 (1998) 267.
[46] R.A. Farrer, B.J. Loughnane, J.T. Fourkas, J. Chem. Phys. 106 (1997) 6901.
[47] A.B. Myers, F. Markel, Chem. Phys. 149 (1990) 21.
[48] N. Pugliano, A.Z. Szarka, S. Gnanakaran, M. Triechel, R. Hochstrasser, J. Chem. Phys. 103 (1995) 6498.
[49] J.T. Fourkas, Laser Phys. 5 (1995) 661.
[50] D.W. Oxtoby, Ann. Rev. Phys. Chem. 32 (1981) 77.
[51] D.W. Oxtoby, Adv. Chem. Phys. 40 (1979) 1.
[52] M. Tuckerman, B.J. Berne, J. Chem. Phys. 98 (1993) 7301.
[53] A.M. Levine, M. Shapiro, E. Pollak, J. Chem. Phys. 88 (1988) 1959.
[54] D.W. Oxtoby, J. Chem. Phys. 70 (1979) 2605.
[55] D.W. Oxtoby, D. Levesque, J.J. Weis, J. Chem. Phys. 68 (1978) 5528.
[56] R.B. Williams, R.F. Loring, J. Chem. Phys. 112 (2000) 3104.
[57] A. Tokmakoff, A.S. Kwok, R.S. Urdahl, R.S. Francis, M.D. Fayer, Chem. Phys. Lett. 234 (1994) 289.
[58] T.W. Pollard, R. Friesner, J. Chem. Phys. 100 (1994) 5054.
[59] J.S. Bader, B.J. Berne, E. Pollack, P. Hanggi, J. Chem. Phys. 104 (1996) 1111.
[60] K. Okumura, A. Tokmakoff, Y. Tanimura, Chem. Phys. Lett. 488 (1999) 488.
[61] A. Tokmakoff, J. Phys. Chem. A 104 (2000) 4247.